International Journal of Solids and Structures 47 (2010) 2600–2612

Contents lists available at ScienceDirect

International Journal of Solids and Structures

journal homepage: www.elsevier.com/locate/ijsolstr

A boundary element formulation for wear modeling on 3D contact and rolling-contact problems

L. Rodríguez-Tembleque [a,1], R. Abascal [a,*], M.H. Aliabadi [b,2]

[a] Escuela Técnica Superior de Ingenieros, Camino de los descubrimientos s/n, 41092 Sevilla, Spain

[b] Department of Aeronautics, Faculty of Engineering, Imperial College, University of London, South Kensington Campus, London SW7 2AZ, UK

ARTICLE INFO

Article history:
Received 1 March 2010
Received in revised form 28 April 2010
Available online 1 June 2010

Keywords:
Wear
Fretting
Contact mechanics
Rolling-contact
Boundary element method

ABSTRACT

The present work shows a new numerical treatment for wear simulation on 3D contact and rolling-contact problems. This formulation is based on the boundary element method (BEM) for computing the elastic influence coefficients and on projection functions over the augmented Lagrangian for contact restrictions fulfillment. The constitutive equations of the potential contact zone are Signorini's contact conditions, Coulomb's law of friction and Holm–Archard's law of wear. The proposed methodology is applied to predict wear on different contact and rolling-contact problems. Results are validated with numerical solutions and semi-analytical models presented in the literature. The BEM considers only the degrees of freedom involved on these kind of problems (those on the solids surfaces), reducing the number of unknowns and obtaining a very good approximation on contact tractions using a low number of elements. Together with the formulation, an acceleration strategy is presented allowing to reduce the times of resolution.

1. Introduction

Wear is one of the main reasons of inoperability in mechanical components, what produces enormous costs. For this reason, and thanks to the advances on measurements techniques, this phenomena was started to be studied in-depth at the end of the first half of the twentieth century. It has to be mentioned the works of Holm (1946) and Archard (1953) which converged to the same wear (by adhesion) model: the *Holm–Archard wear law*. Today, there are more complex and specific wear laws, most of them collected, for example, on Meng's work (Meng, 1994). Even though, the *Holm–Archard wear law* is still valid nowadays for engineering applications. Also, it has to be mentioned the works of Rabinowicz, which are collected on his book (Rabinowicz, 1995), together with the main research about friction and wear.

In the area of numerical simulations, several different formulations, using different methodologies and algorithms, have been proposed for wear prediction. On contact problems, it has to be mentioned the fundamental works of Johansson (1994), Strömbeg et al. (1996), Strömbeg (1997), Christensen et al. (1998), Strömbeg (1999) and Ireman et al. (2003), which present the formulations and fundamentals for wear simulations. The works of Põdra and Andersson (1999a) and Põdra and Andersson (1999b) present a sliding wear algorithm based on the FEM commercial code. On the BEM area, the number of works related with wear is not very ample, the main ones belongs to Sfantos and Aliabadi (2006a), Sfantos and Aliabadi (2006b), Sfantos and Aliabadi (2007) and Lee et al. (2009).

Wear simulation on rolling contact problems on lubricated spherical roller thrust bearings has been tackled by Olofsson et al. (2000). Jendel (2002) proposed a model for predicting wear on train wheel profiles and compares the results with field measurements. That model is completed by Enblom and Berg in their work (Enblom and Mats, 2005). Also it has to be mentioned the works of Telliskivi (2004) and Telliskivi and Olofsson (2004), where a semi-winkler based model is presented and applied to simulate wear on disc-on-disc and wheel-rail. Some of these mentioned models are summarized in De Arizon et al. work (De Arizon et al., 2007). Finally, Hegadekatte et al. (2008) have presented a simplified model (GIWM: *Global Incremental Wear Model*) which allow to estimate the maximum wear depth in *pin on disc* and *twin discs* tribometers, but not the solids profiles and contact pressures evolution.

The methodology suggested in this work for contact modeling is based on an augmented Lagrangian formulation whose precursors are Landers and Taylor (1985), Wriggers et al. (1985), Simo et al. (1985), Alart and Cournier (1991) and Simo and Laursen (1992). The books of Laursen (2002) and Wriggers (2002) compile all this formulations together with the main strategies for numerical contact problems.

* Corresponding author. Tel.: +34 954 487486.
E-mail addresses: abascal@us.es (R. Abascal), m.h.aliabadi@imperial.ac.uk (M.H. Aliabadi).
[1] Tel.: +34 954 487486.
[2] Tel.: +44 (0)20 7594 5077.

0020-7683/$ - see front matter © 2010 Elsevier Ltd. All rights reserved.
doi:10.1016/j.ijsolstr.2010.05.021

The rolling contact formulation is based on Kalker's one, which is collected on his book (Kalker, 1990) or in Johnson's book (Johnson, 1985). This formulation it has been applied on 2D and 3D problems, using the BEM, by González and Abascal (1998), González and Abascal (2000), González and Abascal (2002), Abascal and Rodríguez-Tembleque (2007) and Rodríguez-Tembleque and Abascal (2010), allowing to consider real solid geometries (not only half-spaces) and unstructured meshes. Furthermore, there is a normal and tangential cross-influence relation.

This work presents a new BEM formulation for computing wear on 3D contact and rolling-contact problems. The methodology, based on previous works: (Sfantos and Aliabadi, 2006a; Sfantos and Aliabadi, 2006b; Sfantos and Aliabadi, 2007, uses the BEM for computing the elastic influence coefficients, and on the projection functions over the augmented Lagrangian for contact restrictions fulfilment. The BEM is a very suitable numerical method for this kind of solids mechanical interaction problem, considering only the boundary degrees of freedom involved on the problem, and obtaining a very good approximation on contact tractions. The material loss of the bodies is modeled using the Holm–Archard's linear wear law, which is very extended for many engineering applications. Finally, an acceleration strategy is applied on the algorithm for the resolution of some examples, allowing to obtain a considerable reduction on execution time.

2. Contact model

2.1. Contact kinematics

Let us consider the contact between two solids Ω^α ($\alpha = 1,2$), with boundaries Γ^α, and defined with respect to a Cartesian reference system: $x_i \equiv \{x_1,x_2,x_3\}$ en $\mathbb{R}^3$. The gap variable is defined at all times (τ) for the pair $I \equiv \{P^1,P^2\}$ of points ($P^\alpha \in \Omega^\alpha$, $\alpha = 1,2$), as

$$\mathbf{g} = \mathbf{B}^T(\mathbf{x}^2 - \mathbf{x}^1), \tag{1}$$

where $\mathbf{x}^\alpha$ is the position of P^α at every instant, defined as: $\mathbf{x}^\alpha = \mathbf{X}^\alpha + \mathbf{u}_o^\alpha + \mathbf{u}^\alpha$ ($\mathbf{X}^\alpha$: global position; $\mathbf{u}_o^\alpha$: rigid body global displacement; $\mathbf{u}^\alpha$: elastic displacement expressed in the global system). Matrix $\mathbf{B} = [\mathbf{t}_1|\mathbf{t}_2|\mathbf{n}]$, is a base change matrix expressing the pair I gap in relation to the local orthonormal base $\{\mathbf{t}_1,\mathbf{t}_2,\mathbf{n}\}$ associated to every I pair. The unitary vector $\mathbf{n}$ is normal to the contact surfaces with the same direction as the normal to Γ^1 and expressed in the global system. Vectors $\{\mathbf{t}_1,\mathbf{t}_2\}$ are the tangential unitarian vectors.

The expression (1) can be written as

$$\mathbf{g} = \mathbf{B}^T(\mathbf{X}^2 - \mathbf{X}^1) + \mathbf{B}^T(\mathbf{u}_o^2 - \mathbf{u}_o^1) + \mathbf{B}^T(\mathbf{u}^2 - \mathbf{u}^1), \tag{2}$$

being $\mathbf{B}^T(\mathbf{X}^2 - \mathbf{X}^1)$ the *geometric gap* between two solids in the reference configuration ($\mathbf{g}_g$), and $\mathbf{B}^T(\mathbf{u}_o^2 - \mathbf{u}_o^1)$ the gap originated due to the *rigid body movements* ($\mathbf{g}_o$). Therefore, the gap of the I pair remains as follows:

$$\mathbf{g} = \mathbf{g}_{go} + \mathbf{B}^T(\mathbf{u}^2 - \mathbf{u}^1), \tag{3}$$

where $\mathbf{g}_{go} = \mathbf{g}_g + \mathbf{g}_o$. Two components can be identified on (3): the normal gap, $g_n = g_{go,n} + u_n^2 - u_n^1$, and the tangential gap or *slip*, $\mathbf{g}_t = \mathbf{g}_{go,t} + \mathbf{u}_t^2 - \mathbf{u}_t^1$, being u_n^α and $\mathbf{u}_t^\alpha$ the normal and tangential components of the displacements $\mathbf{u}^\alpha : [\mathbf{u}_t^\alpha u_n^\alpha]^T = \mathbf{B}^T\mathbf{u}^\alpha$.

2.2. Rolling kinematics

The solid particles are traveling through the contact zone because of the solids rotations (see Fig. 1). Therefore, the contact of a pair $I \equiv \{P^1,P^2\}$ has to consider as kinematic variables the *normal gap*, g_n, and the *tangential slip velocity*, $\dot{\mathbf{g}}_t$. Formulating the problem from an Eulerian point of view, like Kalker (1990), the contact pairs

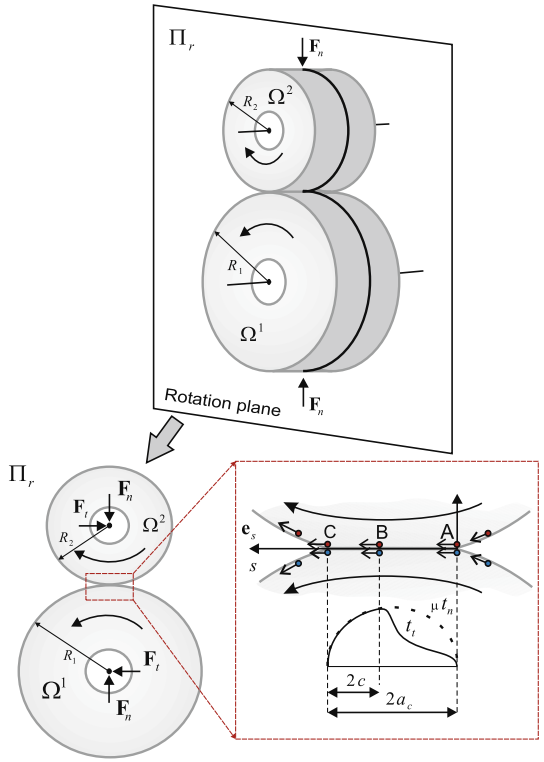

Fig. 1. Rotation plane (Π_r) in which the solids particles trajectories are contained, and solid particles traveling through the rolling-contact region.

relative tangential slip velocities are expressed with respect to a system of reference which travel with the contact zone. Thus the tangential slip velocity can be written as

$$\dot{\mathbf{g}}_t = \frac{d\mathbf{g}_t}{d\tau} = \dot{\mathbf{g}}_{go,t} + (\dot{\mathbf{u}}_t^2 - \dot{\mathbf{u}}_t^1), \tag{4}$$

where $\dot{\mathbf{g}}_{go,t}$ is the *creep*: $\dot{\mathbf{g}}_{go,t} = \mathbf{v}_t^2 - \mathbf{v}_t^1$ (being $\mathbf{v}_t^\alpha$ the tangential velocity of the solid Ω^α particles), and $\dot{\mathbf{u}}_t^\alpha(\alpha = 1,2)$ is the displacement field ($\mathbf{u}_t^\alpha$) material derivative:

$$\dot{\mathbf{u}}_t^\alpha = \frac{\partial \mathbf{u}_t^\alpha}{\partial \tau} + \mathbf{v}_t^\alpha \cdot \nabla \mathbf{u}_t^\alpha. \tag{5}$$

In a rolling without total slip situation, the relative velocities are similar, so ($\mathbf{v}_t^2 \simeq \mathbf{v}_t^1$). Therefore $\|\mathbf{v}_t^2 - \mathbf{v}_t^1\| \ll \|\mathbf{v}_t^2 + \mathbf{v}_t^1\|/2$ (being $\|\cdot\|$ the Euclid's norm), and the expression (5) could be written as:

$$\dot{\mathbf{u}}_t^\alpha = \frac{\partial \mathbf{u}_t^\alpha}{\partial \tau} + \mathbf{v}_t \cdot \nabla \mathbf{u}_t^\alpha, \tag{6}$$

where $\mathbf{v}_t$ is the *mean rolling velocity*: $\mathbf{v}_t = (\mathbf{v}_t^1 + \mathbf{v}_t^2)/2$.

The creep or rigid body tangential slip velocity ($\dot{\mathbf{g}}_{go,t} = \mathbf{v}_t^2 - \mathbf{v}_t^1$) is expressed in the literature (Kalker, 1990) as $\mathbf{c}$:

$$\dot{\mathbf{g}}_{go,t} = \mathbf{c} = \|\mathbf{v}_t\|\boldsymbol{\xi}_t, \tag{7}$$

where ξ_t is the non dimensional creep: $\xi_t = (\mathbf{v}_t^2 - \mathbf{v}_t^1)/\|\mathbf{v}_t\|$.

Defining the operator: $D_r(\cdot) = \partial(\cdot)/\partial\tau + v_{t_1}\partial(\cdot)/\partial x_{t_1} + v_{t_2}\partial(\cdot)/\partial x_{t_2}$ (for the steady state rolling contact: $D_r(\cdot) = v_{t_1}\partial(\cdot)/\partial x_{t_1} + v_{t_2}\partial(\cdot)/\partial x_{t_2}$), the expression (4) can be finally written, according to (6) and (7), as

$$\dot{\mathbf{g}}_t = \mathbf{c} + D_r(\mathbf{u}_t^2 - \mathbf{u}_t^1). \tag{8}$$

2.3. Contact and Rolling-contact laws

The *unilateral contact condition* and the *law of friction* defined for any pair $I \equiv \{P^1,P^2\} \in \Gamma_c$ (Γ_c: *Contact Zone*) of points in contact can be compiled as follows, according to their contact status:

$$\begin{aligned}&\text{Contact-Adhesion}: \quad t_n \leqslant 0;\ g_n = 0;\ \dot{\mathbf{g}}_t = \mathbf{0}\\ &\text{Contact-Slip}: \begin{cases} t_n \leqslant 0; & g_n = 0 \\ \|\mathbf{t}_t\| = \mu|t_n|; & \dot{\mathbf{g}}_t \cdot \mathbf{t}_t = -\|\dot{\mathbf{g}}_t\|\|\mathbf{t}_t\| \end{cases}\\ &\text{No contact}: t_n = 0;\ g_n \geqslant 0;\ \mathbf{t}_t = \mathbf{0}.\end{aligned} \tag{9}$$

In the expression above g_n is the pair I normal gap, and t_n is the normal contact traction defined as

$$t_n = \mathbf{B}_n^T \mathbf{t}^1 = -\mathbf{B}_n^T \mathbf{t}^2, \tag{10}$$

where $\mathbf{t}^\alpha$ is the traction of point $P^\alpha \in \Gamma_c^\alpha$ expressed in the global system of reference, and $\mathbf{B}_n = [\mathbf{n}]$ is the last column in the change of base matrix: $\mathbf{B} = [\mathbf{B}_t|\mathbf{B}_n] = [\mathbf{t}_1|\mathbf{t}_2|\mathbf{n}]$. The normal tractions acting upon the pair I points are of the same value and opposite signs, in accordance with Newton's third law.

In order to approximate the time rate appearing in (9) for contact problems (for rolling-contact it is considered directly from (8)), a simple finite difference is introduced as (Strömbeg, 1997). $\dot{\mathbf{g}}_t$ can be expressed at time τ_k as: $\dot{\mathbf{g}}_t \simeq \Delta\mathbf{g}_t/\Delta\tau$, where $\Delta\mathbf{g}_t = \mathbf{g}_t(\tau_k) - \mathbf{g}_t(\tau_{k-1})$ and $\Delta\tau = \tau_k - \tau_{k-1}$.

2.4. Contact restrictions

For the contact tractions of any I pair of points in contact, the contact laws define a admissible convex region in $\mathbb{R}^3, \mathbb{C}_f$: *Friction Cone*. In order to guarantee that contact traction values remain in C_f, and that (9) is fulfilled, a reformulation of the restrictions is carried out:

$$\mathbf{\Phi}(\mathbf{t}, g_n, \dot{\mathbf{g}}_t) = \mathbf{t} - \mathbb{P}_{\mathbb{C}_f}(\mathbf{t}^*) = \mathbf{0} \tag{11}$$

(augmented Lagrangian contact tractions: $(\mathbf{t}^*)^T = [(\mathbf{t}_t^*)^T t_n^*]$), by means of the following contact operators, presented on Rodríguez-Tembleque and Abascal (2010):

$$\mathbb{P}_{\mathbb{C}_f}(\mathbf{t}^*) = \left\{ \begin{array}{c} \mathbb{P}_{\mathbb{C}_\varrho}(\mathbf{t}_t^*) \\ \mathbb{P}_{\mathbb{R}_-}(t_n^*) \end{array} \right\}. \tag{12}$$

$\mathbb{P}_{\mathbb{R}_-}(t_n^*)$ is the normal projection function acting over the mixed variable or the *augmented normal traction*: $t_n^* = t_n + r g_n (r \in \mathbb{R}_+)$. $\mathbb{P}_{\mathbb{C}_\varrho}(\mathbf{t}_t^*)$ is the tangential projection function acting over the *augmented tangential tractions*: $\mathbf{t}_t^* = \mathbf{t}_t - r\dot{\mathbf{g}}_t$, and over the disc $\mathbb{C}_\varrho$ which radium is: $\varrho = |\mu \mathbb{P}_{\mathbb{R}_-}(t_n^*)|$.

The Eq. (11) compiles the unilateral contact law and the law of friction, taking the following values depending on the rolling contact status of the I pair of points:

- $(t_n^*)_I > 0$ (No Contact): $(\mathbf{t})_I = \mathbf{0}$
- $(t_n^*)_I \leqslant 0$ (Contact):

  [–] $\|(\mathbf{t}_t^*)_I\| < |\mu \mathbb{P}_{\mathbb{R}_-}((t_n^*)_I)|$ (Adhesion): $\left\{ \begin{array}{c} \dot{\mathbf{g}}_t \\ g_n \end{array} \right\}_I = \mathbf{0}.$

  [–] $\|(\mathbf{t}_t^*)_I\| \geqslant |\mu \mathbb{P}_{\mathbb{R}_-}((t_n^*)_I)|$ (Slip): $\left\{ \begin{array}{c} \mathbf{t}_t + \mu t_n^* \boldsymbol{\omega}_t^* \\ g_n \end{array} \right\}_I = \mathbf{0}$

being $\boldsymbol{\omega}_t^* = \mathbf{t}_t^*/\|\mathbf{t}_t^*\|$.

3. Wear model

3.1. Holm–Archard's law

The Holm–Archard's wear law allow to compute the total volume of solid particles worn (W) by *adhesive wear* (Rabinowicz, 1995), as

$$W = k_{ad} \frac{F_n}{H} D_s, \tag{13}$$

where F_n is the contact normal load, H is the surface hardness, D_s is the sliding distance, and k_{ad} is the nondimensional wear coefficient, which represents the probability of forming a substantial wear particle (by interpretation of Archard).

Expression (13) can be written locally for an infinitesimally small apparent contact area as

$$g_w = k_w t_n D_s, \tag{14}$$

being g_w the wear depth, t_n the normal contact pressure, and $k_w = k_{ad}/H$ the dimensional wear coefficient. The total volume worn (W) can be computed integrating the state variable, g_w, on the contact zone:

$$W = \int_{\Gamma_c} g_w d\Gamma. \tag{15}$$

Wear process evolves over time, so Eq. (14) can be expressed in a differential form

$$\dot{g}_w = k_w t_n \dot{D}_s, \tag{16}$$

where $\dot{D}_s$ is the tangential slip velocity module: $\dot{D}_s = \|\dot{\mathbf{g}}_t\|$.

3.2. Wear in contact problems

Considering wear on the contact surfaces, governed by the Holm–Archard's law, the normal contact gap (g_n) is rewritten as

$$g_n = g_{go,n} + (u_n^2 - u_n^1) + g_w \tag{17}$$

for an instant τ_i. For quasi-static contact problems, wear depth defined on instant τ_i, is computed as

$$g_w = g_w(\tau_{k-1}) + k_w t_n \|\Delta\mathbf{g}_t\|, \tag{18}$$

being t_n and $\Delta\mathbf{g}_t$ the normal contact pressure and the sliding distance ($\Delta\mathbf{g}_t = \mathbf{g}_t(\tau_k) - \mathbf{g}_t(\tau_{k-1})$), respectively, calculated on the same instant, and $g_w(\tau_{k-1})$ the wear depth value on instant τ_{k-1}.

Wear depth on each solid surface is computed from the total wear depth g_w as:

$$g_w^1 = \frac{g_w}{1 + (k_w^2/k_w^1)} \quad g_w^2 = \frac{g_w}{1 + (k_w^1/k_w^2)}, \tag{19}$$

so: $g_w = g_w^1 + g_w^2$. $k_w^\alpha (\alpha = 1, 2)$ is the solid Ω^α wear coefficient.

3.3. Wear depth in rolling-contact problems

Wear depth computing on 3D rolling-contact problem is based on the work of Jendel (2002), having the following assumptions:

- Steady-state rolling contact, so the slip velocity (8) uses the stationary operator ($D_r(\cdot) = v_{t_1}\partial(\cdot)/\partial x_{t_1} + v_{t_2}\partial(\cdot)/\partial x_{t_2}$).
- The solid particles trajectories through the contact zone (Γ_c) are straight with direction $\mathbf{e}_s$, being contained on a plane Π_r, as Fig. 1 shows.
- The rolling contact semi-wide is denoted by a_c, and it is different for each rotation plane (Π_r). These semi-wide are modified with the number of rotations (n_r).
- The normal contact pressures (t_n) and the tangential slip velocity field ($\dot{\mathbf{g}}_t$) remain constant while a solid particle travels through the contact zone with direction $\mathbf{e}_s$ and velocity $\mathbf{v}_t$.

Considering these assumptions, the contact pairs come into contact on position ($s = 0$), and during the rolling process, they travel through the contact-stick region (AB line, Fig. 1) and contact-sliding region (BC line).

According to (16), wear depth at instant τ that I pair accumulates from position A, can be expressed as

$$g_w = g_w(\tau_A) + \int_{\tau_A}^{\tau} k_w t_n \|\dot{\mathbf{g}}_t\| d\tau, \quad \tau < \tau_C, \tag{20}$$

being τ_C the instant that I pair leaves the rolling contact zone. In the expression (20), a temporal integration between instant τ_A (pair I comes into contact) and instant τ (pair I is at $s \in [0,2a_c]$ position) is done for computing the wear depth. The term $g_w(\tau_A)$ is the initial wear depth which in general conditions it is not null and comes from the wear depth computed on previous rotations.

The product $\|\dot{\mathbf{g}}_t\| d\tau$ represents the sliding distance of I pair. Therefore, as the particles travels with a known velocity ($\mathbf{v}_t$), the Eq. (20) can be expressed in terms of a spatial integration

$$g_w = g_w(\tau_A) + \int_{S_A}^{S_C} k_w t_n \|\dot{\mathbf{g}}_t\| \frac{ds}{\|\mathbf{v}_t\|}. \tag{21}$$

In this case, the integration limits are: position A ($s = S_A = 0$) and position C ($s = S_C = 2a_c$).

The wear depth obtained on each plane Π_r using (21) modifies the solids geometry profiles on each rotation. For this reason is more appropriated to express g_w as a function of rotation k

$$g_w^{(k)} = g_w^{(k-1)} + \int_{S_A^{(k)}}^{S_C^{(k)}} k_w t_n^{(k)} \|\dot{\mathbf{g}}_t^{(k)}\| \frac{ds}{\|\mathbf{v}_t\|}. \tag{22}$$

The first term on the right hand side express the wear depth caused on the previous rotation, and the second term express the wear caused on k rotation. For the first rotation is assumed: $g_w^{(0)} = 0$.

Spin motion can be considered. In that case, it has to be known the solids particles spin velocity field ($\mathbf{v}_t$), and the solid particles spin trajectory s.

Wear depth on each solid surface is computed from the total wear depth g_w in the same way as contact case, using (19).

4. Discrete equations

4.1. Boundary element method

The BEM formulation for elastic continua Ω with boundary Γ is well known and can be found in many classical texts such as (Brebbia and Dominguez, 1992; Aliabadi, 2002. For a boundary point ($P \in \Gamma$), the *Somigliana identity* can be written as:

$$\mathbf{Cu}(P) + CPV\left\{\int_\Gamma \mathbf{t}^*\mathbf{u}d\Gamma\right\} = \int_\Omega \mathbf{u}^*\mathbf{b}d\Omega + \int_\Gamma \mathbf{u}^*\mathbf{t}d\Gamma, \tag{23}$$

where $\mathbf{u}$, $\mathbf{t}$ and $\mathbf{b}$ are, respectively, the displacements, the boundary tractions and the body forces of Ω. $\mathbf{u}^* = \{u_{ij}^*(P,Q)\}$ is the fundamental solution tensor for displacement, and $\mathbf{t}^* = \{t_{ij}^*(P,Q)\}$ for tractions. Both are solution of Navier's equation at point Q in the ith direction due to a unit load applied at point P in the jth direction. The matrix $\mathbf{C}$ is equal to $\frac{1}{2}\mathbf{I}$ for a smooth boundary Γ, and *CPV {I}* is called the *Cauchy Principal Value* of the integral I. Expressions for the fundamental solution tensors in elastostatics and matrix $\mathbf{C}$ can also be found in Brebbia and Dominguez (1992) and Aliabadi (2002).

Dividing the boundary Γ, into N_e elements, $\Gamma^e \in \Gamma$, so: $\Gamma = \bigcup_{e=1}^{N_e}\Gamma^e$ and $\bigcap_{e=1}^{N_e}\Gamma^e = \emptyset$, the integral Eq. (23) can be written as follows:

$$\mathbf{Cu}(P) + \sum_{e=1}^{N_e}\left\{\int_{\Gamma^e} \mathbf{t}^*\mathbf{u}d\Gamma\right\} = \sum_{e=1}^{N_e}\left\{\int_{\Gamma^e} \mathbf{u}^*\mathbf{t}d\Gamma\right\} \tag{24}$$

in case of absence of body loads ($\mathbf{b} = \mathbf{0}$).

The fields $\mathbf{u}$ and $\mathbf{t}$ are approximated over each element Γ^e using shape functions, as a function of the nodal values ($\mathbf{d}^e$ and $\mathbf{p}^e$): $\mathbf{u} \simeq \hat{\mathbf{u}} = \mathbf{N}\mathbf{d}^e$ and $\mathbf{t} \simeq \hat{\mathbf{t}} = \mathbf{N}\mathbf{p}^e$, being $\mathbf{N}$ the shape function approximation matrix.

After the discretization, the Eq. (24) can be written as

$$\mathbf{C}_i\mathbf{u}_i + \sum_{j=1}^{N}\mathbf{H}_i^e\mathbf{d}^e = \sum_{j=1}^{N}\mathbf{G}_i^e\mathbf{p}^e, \tag{25}$$

being

$$\mathbf{H}_i^e = \int_{\Gamma^e}\mathbf{t}^*\mathbf{N}d\Gamma; \quad \mathbf{G}_i^e = \int_{\Gamma^e}\mathbf{u}^*\mathbf{N}d\Gamma, \tag{26}$$

the integrals over the element e when the collocation point is the node i.

Finally, the contribution for all i nodes can be written together in matrix form to give the global system of equations,

$$\mathbf{Hd} = \mathbf{Gp}, \tag{27}$$

where $\mathbf{d}$ and $\mathbf{p}$ are the displacements and tractions nodal vectors, respectively. Matrices $\mathbf{G}$ and $\mathbf{H}$ are constructed collecting the terms of matrices $\mathbf{H}_i^e$ and $\mathbf{G}_i^e$.

Assuming that the displacement or the traction is known on each node and direction, the boundary conditions can be imposed rearranging the columns in $\mathbf{H}$ and $\mathbf{G}$, and passing all the unknowns to vector $\mathbf{x}$ on the left hand side. This gives the final system of equations:

$$\mathbf{Ax} = \mathbf{F}. \tag{28}$$

4.2. Contact discrete variables

To consider the contact between two solids, the contact tractions ($\mathbf{t}_c$), the gap ($\mathbf{g}$) the tangential slip velocity ($\dot{\mathbf{g}}_t$), and the solids displacements ($\mathbf{u}^\alpha$, $\alpha = 1, 2$), are discretized over the contact interface (Γ_c). To that end, Γ_c is divided into N_e^f elemental surfaces (Γ_c^e), thus: $\Gamma_c = \bigcup_{e=1}^{N_e^f}\Gamma_c^e$ and $\bigcap_{e=1}^{N_e^f}\Gamma_c^e = \emptyset$. These elements ($\Gamma_c^e$) constitute a *contact frame*.

The contact tractions are discretized over the contact frame as: $\mathbf{t}_c \simeq \hat{\mathbf{t}}_c = \sum_{i=1}^{N^f}\delta_{P_i}\boldsymbol{\lambda}_i$, where δ_{P_i} is the Dirac's delta on each contact frame node i, and $\boldsymbol{\lambda}_i$ is the Lagrange multiplier on the node ($i = 1,\ldots,N^f$). The gap ($\mathbf{g}$) is approximated in the same way: $\mathbf{g} \simeq \hat{\mathbf{g}} = \sum_{i=1}^{N^f}\delta_{P_i}\mathbf{k}_i$, where $\mathbf{k}_i$ is the nodal value. The tangential slip velocity approximation will be described in details in the next section: $\dot{\mathbf{g}} \simeq \mathbf{s}_t$.

The discrete expression of Eq. (3) can be written as:

$$\mathbf{k} = \mathbf{C}_g\mathbf{k}_{go} + (\mathbf{C}^2)^T\mathbf{x}^2 - (\mathbf{C}^1)^T\mathbf{x}^1, \tag{29}$$

being $\mathbf{k}$ the contact pairs gap vector and $\mathbf{k}_{go}$ the initial geometrical gap and rigid body movement vector. The matrices $\mathbf{C}^\alpha$ ($\alpha = 1, 2$) and $\mathbf{C}_g$ are defined as $\mathbf{C}^\alpha = \sum_{i=1}^{N^\alpha}\sum_{j=1(i,j)\equiv I}^{N^f}(\mathcal{L}_i^\alpha)^T\mathbf{B}_j\mathcal{L}_j^f$ and $\mathbf{C}_g = \sum_{i=1}^{N^f}\sum_{j=1(i,j)\equiv I}^{N^f}(\mathcal{L}_i^f)^T\mathcal{L}_j^f$, where $\mathcal{L}_i^\alpha$ and $\mathcal{L}_i^f$ are Boolean assembling operators: $\mathbf{d}_i^\alpha = \mathcal{L}_i^\alpha\mathbf{x}^\alpha$ and $\boldsymbol{\lambda}_i = \mathcal{L}_i^f\boldsymbol{\Lambda}$. Matrix operator $\mathcal{L}_i^\alpha$ allows to extract the contact node i displacement ($\mathbf{d}_i^\alpha$), from vector $\mathbf{x}^\alpha$, and $\mathcal{L}_i^f$ extracts from the multipliers vector ($\boldsymbol{\Lambda}$), the variable associated to node i ($\boldsymbol{\lambda}_i$). Vector $\mathbf{x}^\alpha$ is organized as $(\mathbf{x}^\alpha)^T = \left[(\mathbf{x}_p^\alpha)^T(\mathbf{d}_c^\alpha)^T\right]$ ($\mathbf{x}_p^\alpha$: external unknowns; $\mathbf{d}_c^\alpha$: contact displacement unknowns), so matrix $\mathbf{C}^\alpha$ has the following structure: $(\mathbf{C}^\alpha)^T = [\mathbf{0}(\widetilde{\mathbf{C}}^\alpha)^T]$. The matrix $\mathbf{C}_g$ is equal to the identity matrix: $\mathbf{C}_g = \mathbf{I}$.

4.3. BEM–BEM coupling

In case of modeling the solids $\Omega^\alpha(\alpha = 1, 2)$ using the BEM (28), the solids coupling equations set can be expressed as:

$$\begin{bmatrix} \mathbf{A}_x^1 & \mathbf{0} & \mathbf{A}_p^1\widetilde{\mathbf{C}}^1 & \mathbf{0} \\ \mathbf{0} & \mathbf{A}_x^2 & -\mathbf{A}_p^2\widetilde{\mathbf{C}}^2 & \mathbf{0} \\ (\mathbf{C}^1)^T & -(\mathbf{C}^2)^T & \mathbf{0} & \mathbf{C}_g \end{bmatrix} \begin{Bmatrix} \mathbf{x}^1 \\ \mathbf{x}^2 \\ \mathbf{\Lambda} \\ \mathbf{k} \end{Bmatrix} = \begin{Bmatrix} \mathbf{F}^1 \\ \mathbf{F}^2 \\ \mathbf{C}_g\mathbf{k}_{go} \end{Bmatrix}, \tag{30}$$

being vector $\mathbf{\Lambda}$ the nodal contact tractions, so that: $\mathbf{p}_c^1 = \widetilde{\mathbf{C}}^1\mathbf{\Lambda}$ and $\mathbf{p}_c^2 = -\widetilde{\mathbf{C}}^2\mathbf{\Lambda}$.

The first two rows on (30) represents the boundary element equations of each solid, and the third row, the kinematic contact equations. Eq. (30) can be written in a more compact form as:

$$\mathbf{R}^1\mathbf{x}^1 + \mathbf{R}^2\mathbf{x}^2 + \mathbf{R}_\lambda\mathbf{\Lambda} + \mathbf{R}_g\mathbf{k} = \mathbf{F}, \tag{31}$$

being,

$$\mathbf{R}^1 = \begin{bmatrix} \mathbf{A}^1 \\ \mathbf{0} \\ (\mathbf{C}_1)^T \end{bmatrix}, \quad \mathbf{R}^2 = \begin{bmatrix} \mathbf{0} \\ \mathbf{A}^2 \\ -(\mathbf{C}_2)^T \end{bmatrix}, \quad \mathbf{R}_\lambda = \begin{bmatrix} \mathbf{A}_p^1\widetilde{\mathbf{C}}_1 \\ -\mathbf{A}_p^2\widetilde{\mathbf{C}}_2 \\ \mathbf{0} \end{bmatrix}, \quad \mathbf{R}_g = \begin{bmatrix} \mathbf{0} \\ \mathbf{0} \\ \mathbf{C}_g \end{bmatrix}, \quad \mathbf{F} = \begin{bmatrix} \mathbf{F}^1 \\ \mathbf{F}^2 \\ \mathbf{C}_g\mathbf{k}_{go} \end{bmatrix}. \tag{32}$$

4.4. Tangential slip velocity approximation

The tangential slip velocity Eq. (8) could be discretized and expressed according to Rodríguez-Tembleque and Abascal (2010) as:

$$\mathbf{s}_t = \bar{\mathbf{c}} + \widetilde{\mathbf{D}}_r\mathbf{k}, \tag{33}$$

where $\mathbf{s}_t$ is a vector which stores the slip velocity of every contact pair $I (I = 1, \ldots, N_p)$, $\bar{\mathbf{c}}$ is a vector which stores the creep velocities, and the vector $\mathbf{k} = \mathbf{k}_{go} + (\mathbf{C}^2)^T\mathbf{x}^2 - (\mathbf{C}^1)^T\mathbf{x}^1$, stores the gap of every contact pair:

$$\mathbf{s}_t = \begin{bmatrix} (\mathbf{s}_t)_1 \\ \vdots \\ (\mathbf{s}_t)_I \\ \vdots \\ (\mathbf{s}_t)_{N_p} \end{bmatrix} \quad \bar{\mathbf{c}} = \begin{bmatrix} \bar{\mathbf{c}}_1 \\ \vdots \\ \bar{\mathbf{c}}_I \\ \vdots \\ \bar{\mathbf{c}}_{N_p} \end{bmatrix} \quad \mathbf{k} = \begin{bmatrix} (\mathbf{k})_1 \\ \vdots \\ (\mathbf{k})_I \\ \vdots \\ (\mathbf{k})_{N_p} \end{bmatrix}, \tag{34}$$

$$\mathbf{k}_I = \begin{bmatrix} \mathbf{k}_t \\ k_n \end{bmatrix}_I = \begin{bmatrix} \mathbf{0} \\ k_{go,n} \end{bmatrix}_I + \begin{bmatrix} \mathbf{d}_t^2 \\ d_n^2 \end{bmatrix}_I - \begin{bmatrix} \mathbf{d}_t^1 \\ d_n^1 \end{bmatrix}_I.$$

Finally, $\widetilde{\mathbf{D}}_r$ is a $2N_p \times 3N_p$ square matrix defined in Rodríguez-Tembleque and Abascal (2010):

$$\widetilde{\mathbf{D}}_r = \begin{bmatrix} (d_r)_{11}[\mathbf{I}\ \mathbf{0}] & \ldots & (d_r)_{1N_p}[\mathbf{I}\ \mathbf{0}] \\ \vdots & \ddots & \vdots \\ (d_r)_{N_p1}[\mathbf{I}\ \mathbf{0}] & \ldots & (d_r)_{N_pN_p}[\mathbf{I}\ \mathbf{0}] \end{bmatrix}, \tag{35}$$

so $\widetilde{\mathbf{D}}_r\mathbf{k}$ approximates the convective term in (8), for the steady-state case, using a *Least-squares technique*.

4.5. Wear equations for contact problems

The wear depth for every instant or rotation $\left(g_{\mathrm{w}}^{(k)}\right)$ can be discretized over de contact frame, as a function of the nodal values. Therefore the wear variable is approximated over each contact frame element as

$$g_{\mathrm{w}}^{(k)} \simeq \hat{g}_{\mathrm{w}}^{(k)} = \widetilde{\mathbf{N}}\mathbf{w}^e, \tag{36}$$

where $\widetilde{\mathbf{N}}$ is the shape functions matrix defined for the frame element Γ_c^e, and $\mathbf{w}^e$ is the nodal wear depth vector of element Γ_c^e.

The discrete form of kinematic Eq. (17) for I pair, on instant k, is:

$$\left(\mathbf{k}^{(k)}\right)_I = \left(\mathbf{k}_{go}^{(k)}\right)_I + \left(\mathbf{d}^{2\,(k)}\right)_I - \left(\mathbf{d}^{1\,(k)}\right)_I + \left(\mathbf{C}_{gn}\mathbf{w}^{(k)}\right)_I, \tag{37}$$

where matrix $\mathbf{C}_{gn}$ is constituted of the $\mathbf{C}_g$ columns which affect the normal gap of contact pairs, and $\mathbf{w}^{(k)}$ is a vector which contains the contact pairs wear depth.

According to the Holm–Archard's law (16), wear is caused by the tangential slip ratio or the tangential slip velocity. In case of a contact problem, the discrete for of Expression (18) can be expressed for I pair as

$$\begin{aligned} \left(\mathbf{w}^{(k)}\right)_I &= \left(\mathbf{w}^{(k-1)}\right)_I + \left(\Delta\mathbf{w}^{(k)}\right)_I, \\ \left(\Delta\mathbf{w}^{(k)}\right)_I &= k_{\mathrm{w}}\left(\mathbf{\Lambda}_n^{(k)}\right)_I \left\| \left(\mathbf{k}_t^k\right)_I - \left(\mathbf{k}_t^{(k-1)}\right)_I \right\|, \end{aligned} \tag{38}$$

where $\mathbf{\Lambda}_n^{(k)}$ is a vector which contains the normal traction components of contact pairs at instant k.

4.6. Wear equations for rolling-contact problems

Rolling-contact problem considers an Eulerian formulation. So the wear depth increment on every rolling plane, Π_r, is computed according to (22), as:

$$\begin{aligned} \left(\mathbf{w}^{(k)}\right)_I &= \left(\mathbf{w}^{(k-1)}\right)_I + \left(\Delta\mathbf{w}^{(k)}\right)_{\Pi_r}, \\ \left(\Delta\mathbf{w}^{(k)}\right)_{\Pi_r} &= \sum_{I=\{I\in\Gamma_c\cap\Pi_r\}}^{N_I} \Delta\tau k_{\mathrm{w}}\left(\mathbf{\Lambda}_n^{(k)}\right)_I \left\| \left(\mathbf{s}_t^{(k)}\right)_I \right\|, \end{aligned} \tag{39}$$

being I the contact pairs on Π_r, and $(\mathbf{s}_t^{(k)})_I$ their tangential slip velocity:

$$\left(\mathbf{s}_t^{(k)}\right)_I = (\bar{\mathbf{c}})_I + \left(\widetilde{\mathbf{D}}_r\mathbf{k}^{(k)}\right)_I, \tag{40}$$

$\Delta\tau$is the time spent by a solid particle traveling from one node to the consecutive one in direction $\mathbf{e}_s$ (the nodes in direction $\mathbf{e}_s$ have equidistant positions, Fig. 2). Its value is

$$\Delta\tau = T/N_I, \tag{41}$$

where T is the residence time of a solid particle in the potential contact zone, and N_I the number of nodes in $\mathbf{e}_s$ direction.

The residence time is computed from the potential contact zone width $2\hat{a}_c$ and the rolling velocity $\mathbf{v}_t$, as:

$$T = 2\hat{a}_c/\|\mathbf{v}_t\|. \tag{42}$$

4.7. Rolling contact restrictions

The contact restrictions for every I pair, at instant k can be expressed as:

$$\left(\mathbf{\Lambda}_n^{*(k)}\right)_I - \mathbb{P}_{\mathbb{R}_-}\left(\left(\mathbf{\Lambda}_n^{*(k)}\right)_I\right) = 0 \quad \left(\mathbf{\Lambda}_t^{*(k)}\right)_I - \mathbb{P}_{C_\varrho}\left(\left(\mathbf{\Lambda}_t^{*(k)}\right)_I\right) = \mathbf{0}. \tag{43}$$

The augmented contact variables are defines as: $\mathbf{\Lambda}_n^{*(k)} = \mathbf{\Lambda}_n^{(k)} + r_n\mathbf{k}_n^{(k)}$ and $\mathbf{\Lambda}_t^{*(k)} = \mathbf{\Lambda}_t^{(k)} - r_t\left(\mathbf{k}_t^{(k)} - \mathbf{k}_t^{(k-1)}\right)$, and the rolling contact ones, as: $\mathbf{\Lambda}_n^{*(k)} = \mathbf{\Lambda}_n^{(k)} + r_n\mathbf{k}_n^{(k)}$ and $\mathbf{\Lambda}_t^{*(k)} = \mathbf{\Lambda}_t^{(k)} - r_t\mathbf{s}_t^{(k)}$. The value of friction limit, ϱ, for the tangential projection function (12), on I pair, is: $\varrho = \mu\left|\mathbb{P}_{\mathbb{R}_-}\left(\left(\mathbf{\Lambda}_n^{*(k)}\right)_I\right)\right|$ or $\varrho = \mu\left|\mathbb{P}_{\mathbb{R}_-}\left(\left(\mathbf{\Lambda}_n^{(k)}\right)_I\right)\right|$.

5. Resolution algorithm

5.1. Contact problems

The quasi-static contact problem considering wear (31), (32), (37), (38) and (43) is solved as follows. The variables on instant $(k-1)$ are known, and the instant (k) unknowns, $\mathbf{z}^{(k)} = [(\mathbf{x}^1)^T(\mathbf{x}^2)^T$

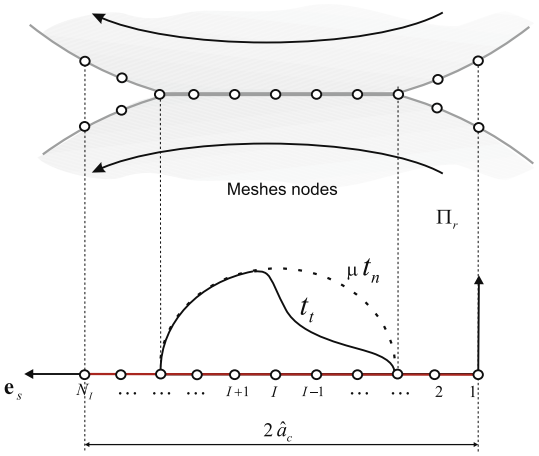

Fig. 2. Equidistant distribution of nodes on plane (Π_r).

$\mathbf{\Lambda}^T\mathbf{k}^T\mathbf{w}^T]$, are computed using the following iterative Uzawa scheme with index (n):

(I) Apply the rigid body rapprochement increment: $\Delta\mathbf{k}_o^{(n)} < 0$.
(II) Initialize all the contact pair tractions and their wear depth:

$$\left(\mathbf{\Lambda}^{(n)}\right)_I = \left(\mathbf{\Lambda}^{(k-1)}\right)_I, \quad \left(\mathbf{w}^{(n)}\right)_I = \left(\mathbf{w}^{(k-1)}\right)_I, \quad \left(\Delta\mathbf{w}^{(n)}\right)_I = 0. \tag{44}$$

(III) Solve the linear equations set:

$$\begin{bmatrix}\mathbf{R}^1 & \mathbf{R}^2 & \mathbf{R}_g\end{bmatrix}\begin{bmatrix}\mathbf{x}^1\\ \mathbf{x}^2\\ \mathbf{k}\end{bmatrix}^{(n)} = -\mathbf{R}_\lambda\mathbf{\Lambda}^{(n)} + \begin{bmatrix}\mathbf{F}^{1(k)}\\ \mathbf{F}^{2(k)}\\ \mathbf{k}_g + \mathbf{k}_o^{(n-1)} + \Delta\mathbf{k}_o^{(n)} + \mathbf{C}_{g_n}\mathbf{w}^{(n)}\end{bmatrix}. \tag{45}$$

(IV) Compute the contact tractions, $\mathbf{\Lambda}^{(n+1)}$, and the wear increment, $\Delta\mathbf{w}^{(n+1)}$, for every contact pair I:

$$\left(\mathbf{\Lambda}_n^{(n+1)}\right)_I = \mathbb{P}_{\mathbb{R}_-}\left(\left(\mathbf{\Lambda}_n^{(n)}\right)_I + r_n\left(\mathbf{k}_n^{(n)}\right)_I\right), \tag{46}$$

$$\left(\mathbf{\Lambda}_t^{(n+1)}\right)_I = \mathbb{P}_{C_\varrho}\left(\left(\mathbf{\Lambda}_t^{(n)}\right)_I - r_t\left[\left(\mathbf{k}_t^{(n)}\right)_I - \left(\mathbf{k}_t^{(k-1)}\right)_I\right]\right), \tag{47}$$

being $\varrho = \mu|(\mathbf{\Lambda}_n^{(n+1)})_I|$, and

$$\begin{aligned}\left(\Delta\mathbf{w}^{(n)}\right)_I &= k_w\left(\mathbf{\Lambda}_n^{(n+1)}\right)_I\left\|\left(\mathbf{k}_t^{(n)} - \mathbf{k}_t^{(k-1)}\right)_I\right\|,\\ \left(\mathbf{w}^{(n+1)}\right)_I &= \left(\mathbf{w}^{(n)}\right)_I + \left(\Delta\mathbf{w}^{(n)}\right)_I.\end{aligned} \tag{48}$$

(V) Compute the error function:

$$\Psi\left(\mathbf{\Lambda}^{(n+1)}\right) = \left\|\mathbf{\Lambda}^{(n+1)} - \mathbf{\Lambda}^{(n)}\right\|. \tag{49}$$

(a) If $\Psi(\mathbf{\Lambda}^{(n+1)}) \leqslant \varepsilon$, the solution for the instant (k): $\mathbf{z}^{(k)} = \mathbf{z}^{(n+1)}$. In case the applied boundary condition is the external load i-component $\left(\mathbf{Q}_i^{(k)}\right)$, before reaching the solution for instant (k), the resultant applied loads on the contact zone (Γ_c) have to be calculated:

$$\mathbf{Q}_i^{(n+1)} = \int_{\Gamma_c}\mathbf{\Lambda}_i^{(n+1)}d\Gamma, \tag{50}$$

(a.1) If $\left|\mathbf{Q}_i^{(n+1)}\right| > \left|\mathbf{Q}_i^{(k)}\right| + \varepsilon_{load}$, modify $\Delta\mathbf{k}_o^{(n)}$ and return to (II).
(a.2) Otherwise, the solution for instant (k) is reached: $\mathbf{z}^{(k)} = \mathbf{z}^{(n+1)}$.
(b) Otherwise, return to (III) evaluating: $\mathbf{\Lambda}^{(n)} = \mathbf{\Lambda}^{(n+1)}$ and $\mathbf{w}^{(n)} = \mathbf{w}^{(n+1)}$, and iterate until the convergence is reached.

After the solution at instant (k), $\mathbf{z}^{(k)}$, is reached, the solution for the next instant is achieved evaluating: $\mathbf{z}^{(k-1)} = \mathbf{z}^{(k)}$ and returning to (I).

5.2. Rolling-contact problems

Wear simulation in steady-state rolling-contact problems computes the wear depth on solids profiles for rotation (k), considering (31) and (32) and (39)–(43). In this case we solve the variables, $\mathbf{z}^T = [(\mathbf{x}^1)^T(\mathbf{x}^2)^T\mathbf{\Lambda}^T\mathbf{k}^T\mathbf{s}_t^T\mathbf{w}^T]$, on rotation (k), from the known values on the previous rotation $(k-1)$.

The solving scheme is the same but on the step (IV), the expressions are:

$$\left(\mathbf{s}_t^{(n)}\right)_I = (\bar{\mathbf{c}})_I + \left(\widetilde{\mathbf{D}}_t\mathbf{k}^{(n)}\right)_I, \tag{51}$$

$$\left(\mathbf{\Lambda}_n^{(n+1)}\right)_I = \mathbb{P}_{\mathbb{R}_-}\left(\left(\mathbf{\Lambda}_n^{(n)}\right)_I + r_n\left(\mathbf{k}_n^{(n)}\right)_I\right) \tag{52}$$

$$\left(\mathbf{\Lambda}_t^{(n+1)}\right)_I = \mathbb{P}_{C_\varrho}\left(\left(\mathbf{\Lambda}_t^{(n)}\right)_I - r_t\left(\mathbf{s}_t^{(n)}\right)_I\right), \tag{53}$$

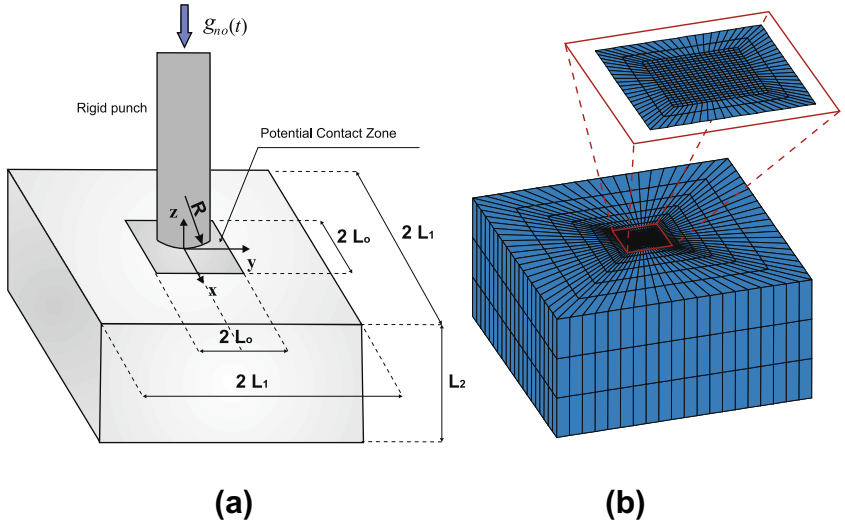

Fig. 3. (a) Problem sketch. (b) Boundary element mesh details.

being $\varrho = \mu|(\boldsymbol{\Lambda}_n^{(n+1)})_I|$, and

$$\begin{aligned}\left(\Delta\mathbf{w}^{(n)}\right)_{\Pi_r} &= \sum_{I=\{I\in\Gamma_c\cap\Pi_r\}}^{N_I}\Delta t\left(k_w\left(\boldsymbol{\Lambda}_n^{(n+1)}\right)_I\left\|\left(\mathbf{s}_t^{(n)}\right)_I\right\|\right)\\ \left(\mathbf{w}^{(n+1)}\right)_I &= \left(\mathbf{w}^{(n)}\right)_I + \left(\Delta\mathbf{w}^{(n)}\right)_{\Pi_r}\end{aligned} \tag{54}$$

The presented algorithm can be accelerated using a fictitious wear coefficient (k_w), what leads to a fictitious wear depth increment, reducing considerably the number of revolutions. This idea was proposed by Strömbeg (1997) for FEM fretting problems, and can be applied on rolling-contact problems with satisfactory results, as the results will show.

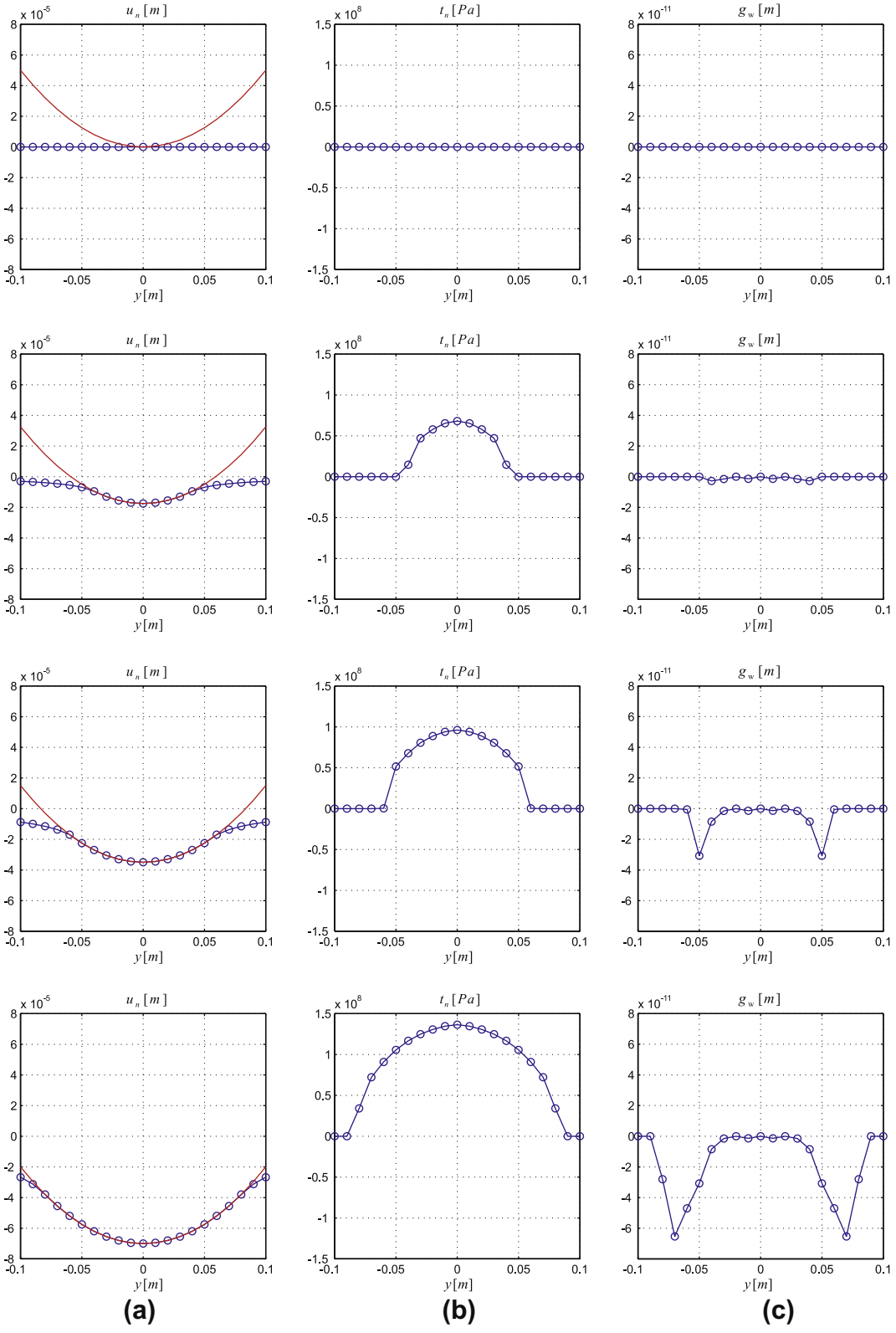

Fig. 4. Magnitudes on plane $x = 0$: (a) Normal elastic displacement u_n. (b) Normal contact traction t_n. (c) Wear depth g_w on the solid surface, for load steps: 0, 10, 20 and 40.

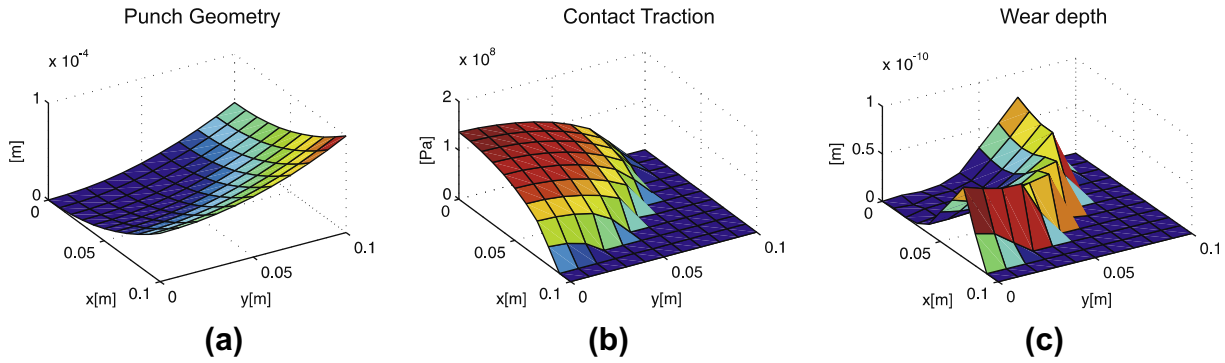

Fig. 5. (a) Initial geometrical gap. (b) Resulting normal contact traction distribution. (c) Resulting wear depth distribution.

6. Numerical examples

The objective of the numerical examples is to show the excellent capabilities of this 3D boundary elements methodology proposed.

6.1. Punch indentation problem

This example was presented by Strömbeg (1999) and deals with wear originated on an elastic tetrahedral by a rigid punch indentation. Wear is caused by the relative tangential slip between solids. This example allow us to validate the boundary element formulation and the algorithm proposed, applied to fretting problems.

Fig. 3a shows the problem sketch. The tetrahedral dimensions are: $L_o = 0.1$ m and $L_1 = L_2 = 1$ m. The domain is discretized by linear quadrilateral boundary elements, using 20×20 elements on the potential contact zone, as Fig. 3b shows.

The material properties are: Young module $E = 210$ GPa and Poisson coefficient $v = 0.3$. The coefficient of friction considered is $\mu = 0.3$, and the wear coefficient $k_w = 1.0 \times 10^{-11}$ Pa^{-1}.

The rigid punch has a radii $R = 100$ m, and causes and indentation of 0.07 mm on 40 load steps. On Fig. 4 we can see the evolution on plane $x = 0$ of: normal elastic displacements (u_n), normal contact tractions (t_n) and wear depth (g_w) on the tetrahedral contact area. Wear appears on the sliding zones. Fig. 5 shows, on a quarter of the contact zone, the initial geometrical gap, $5 \times 10^{-3}(x^2 + y^2)$ m, the resulting normal contact traction distribution, and the resulting wear depth distribution. Results present an excellent agreement with Strömberg solution in Strömbeg (1999).

The evolution of the wear depth and normal contact pressures in a fretting process is illustrated in Fig. 6. The initial geometrical gap is: $0.75(x^4 + y^4)$ m, the coefficient of wear is $k_w = 1.0 \times 10^{-8}$ Pa^{-1}. The punch is indented 0.07 mm during 500 cycles using 20 increments for each cycle. As in Strömbeg (1999), after 500 cy-

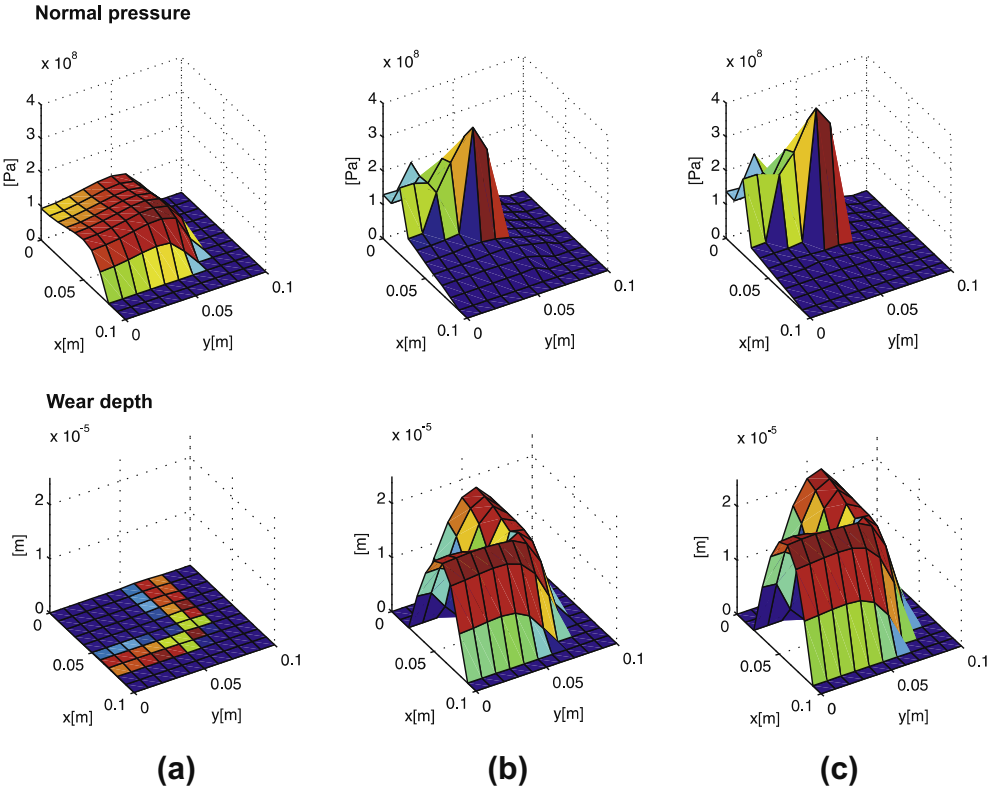

Fig. 6. Normal pressure and wear depth after: (a) 1 load cycle, (b) 250 cycles, and (c) 500 cyles.

cles, the wear depth is developed in the slipping region and contact pressure is turned toward a value of zero. In the sticking zone a hump in the contact pressure is developed, almost a four times greater maximum value than the maximum in the first cycle.

6.2. Pin on disc sliding wear

Tribometers can be applied on the study of wear in complex micro-mechanical components, apart from measure the friction and sliding wear properties of dry or lubricated surfaces of a variety of materials.

This example presents the classic test of a pin on a rotating disc (see Fig. 7a). In this problem the disc is assumed to be very hard and its wear can be neglected compared to the pin wear. If the pin is far from the disc axis and the contact zone is small, the tangential slip velocity is constant and uniform during the wear process. So all the points in the contact zone travel the same distance.

This problem has an analytical solution which has a very good agreement with the experiments of Põdra and Andersson (1999a), and the numerical simulations of Põdra and Andersson (1999a), Sfantos and Aliabadi (2006a), Sfantos and Aliabadi (2006b) and Sfantos and Aliabadi (2007). This solution considers, under the previous paragraph assumptions, the worn volume is a spherical ended pin (see Fig. 7b), which expression is

$$W = \frac{\pi}{3}(3R - \mathrm{w})(\mathrm{w})^2, \tag{55}$$

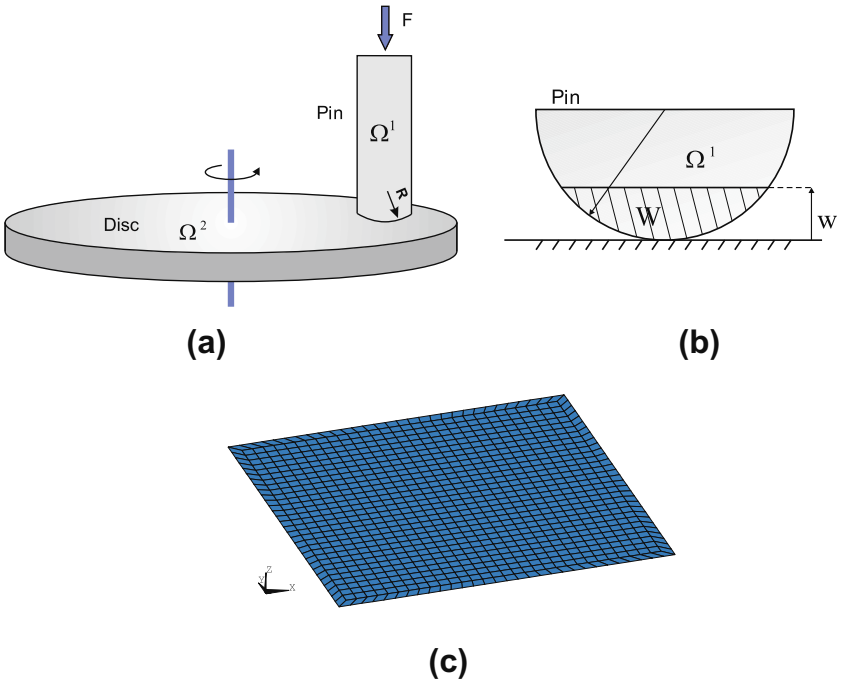

Fig. 7. (a) Elastic pin on a rotatory disc. (b) Pin wear volume (W) and pin maximum wear depth (w). (c) Elastic half-space boundary elements mesh detail.

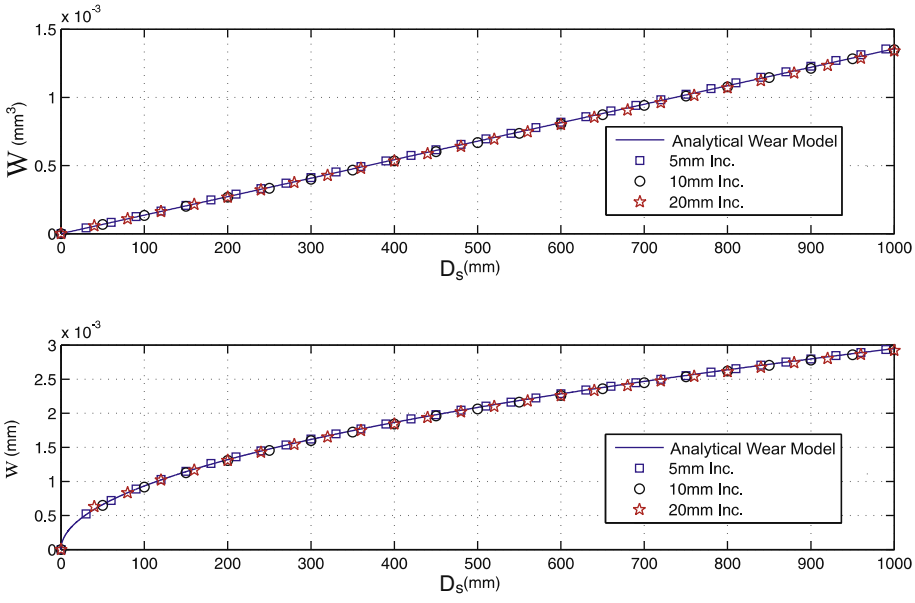

Fig. 8. Wear volume (W) and maximum wear depth (w) during sliding; proposed formulation using different sliding increments compared with analytical model.

where R is the pin radii and w is the wear depth. Using the Holm–Archard's law Eq. (13), the wear depth w can be computed for every sliding distance, solving (55).

The pin and disc material Young's modulus and Poisson's ratio are, respectively: 210 GPa and 0.3, being the wear coefficient 1.33×10^{-13} Pa^{-1}. The pin, whose radius is 50 mm, is subjected to a normal load of 10.2 N. During the numerical simulation the friction is neglected ($\mu = 0.0$), and the sliding increment is considered constant: $\left\| \left(\mathbf{k}_t^{(n)} - \mathbf{k}_t^{(k-1)} \right)_I \right\| = ds$.

For simplicity, the solids are modeled assuming classical approach, using a 30×30 linear quadrilateral 4-node boundary elements mesh in the potential contact zone (see Fig. 7c). A solids half-space approximation is used to compare the contact tractions distributions with classical solutions. During the wear simulation the worn volume is computed considering each element wear contribution, as

$$W = \sum_{\substack{e\text{-element} \\ \text{on } \Gamma_c}} \left\{ \int_{\Gamma_c^e} \mathbf{N}^e d\Gamma \right\} \mathbf{w}^e, \tag{56}$$

where $\mathbf{w}^e$ is the nodal wear depth vector of the e-element.

The results obtained in this example are shown in Figs. 8 and 9. In the first one the volume worn and the wear depth evolution during the sliding distance are shown. The results are computed using different sliding increments, (ds = 5 mm, 10 mm and 20 mm), and compared with the analytical solution. The results have a high agreement with the analytical model presented in Põdra and Andersson (1999a). Increasing ds values, a time reduction on wear simulation is obtained.

Fig. 9a shows the $y = 0$ plane pin profile during wear simulation while Fig. 9b shows the normal pressure distribution. We can see that the initial normal tractions distribution is equal to Hertz pressure, being different as the sliding distance (D_s) increases. Normal pressure decreases its value as the contact zone grows.

If the disc is considered to be worn, and according to (19), after 500 mm of sliding distance the resulting pin and disc profiles are showed in Fig. 10, for solids wear coefficient relations: $k_w^p = k_w^d = 0.665 \times 10^{-13}$ Pa^{-1} (a) and $k_w^p = 2k_w^d = 0.887 \times 10^{-13}$ Pa^{-1} (b).

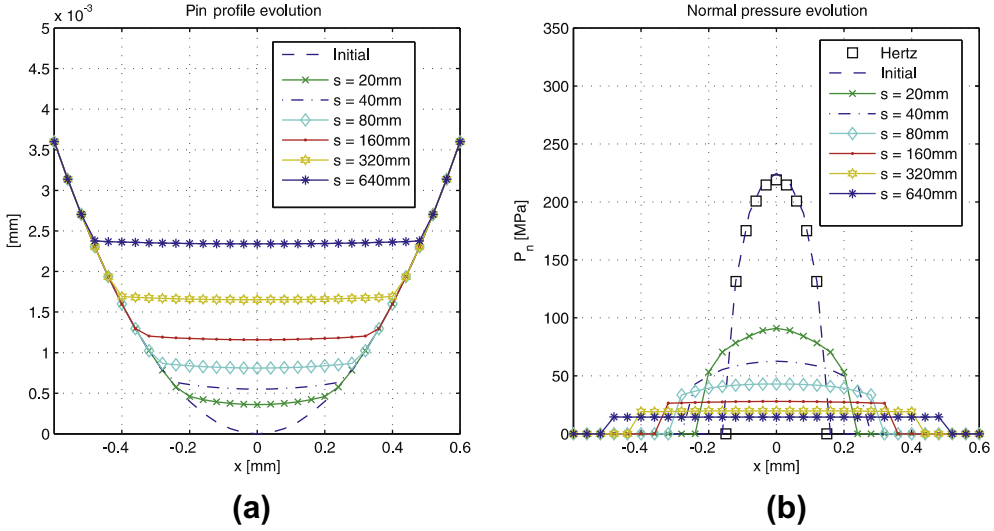

Fig. 9. (a) Pin profile on $y = 0$ evolution during wear simulation. (b) Normal contact pressure distribution evolution.

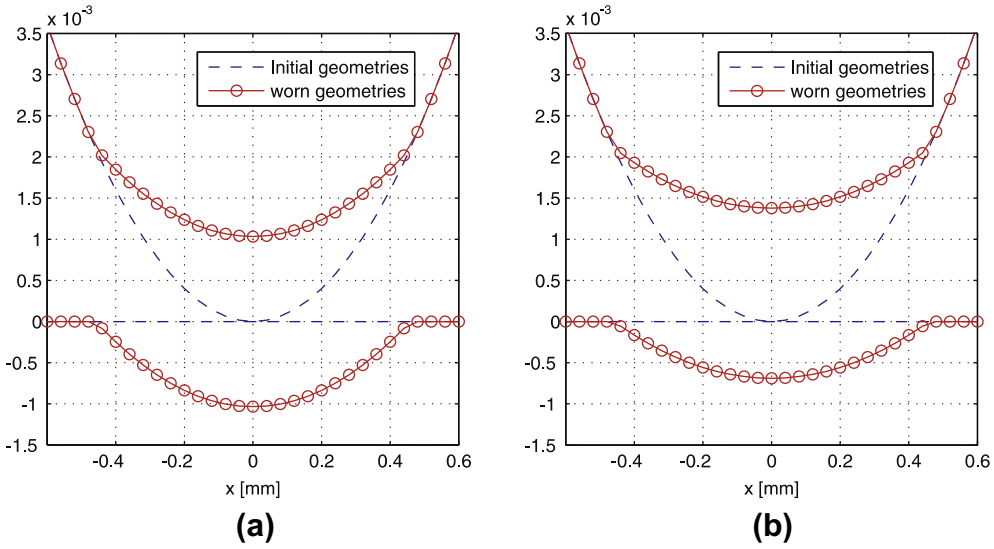

Fig. 10. Pin on disc initial and wear cross-section profiles for the cases: (a) $k_w^p = k_w^d$ and (b) $k_w^p = 2k_w^d$.

6.3. Rolling twin discs

This tribometer system allow to study friction and wear on rolling contact and rolling/sliding contact situations, like in gears or tooth flanks rolling and sliding one against each other.

Fig. 11 shows the twin-disc tribometer system details and the boundary element solid meshes. The solids are approximated by an elastic half-spaces, discretizing the boundary with linear quadrilateral elements.

The applied normal force is $F = 300$ N, the rotation velocity is $\omega = 300$ rev/min, and two creep situations are considered: *Creep* = 0.5% and 1.5%. The discs geometric parameters are: $R11 = 32.5$ mm, $R1 = 125$ mm and $R2 = 32.3$ mm, the materials properties: $E_1 = E_2 = 208 \times 10^3$ N/mm^2 and $\nu_1 = \nu_2 = 0.3$, $\mu = 0.6$, and the wear coefficient: $k_w = 2 \times 10^{-6}$ MPa^{-1}.

The maximum wear depth of this problem can be computed also using the GIWM presented by Hegadekatte et al. (2008), which has been tested satisfactorily with experiments. Fig. 12 shows the very good agreement between the total maximum wear depth evolutions, during 30,000 rotations, obtained for the two creep cases by the GIWM and the BEM formulation.

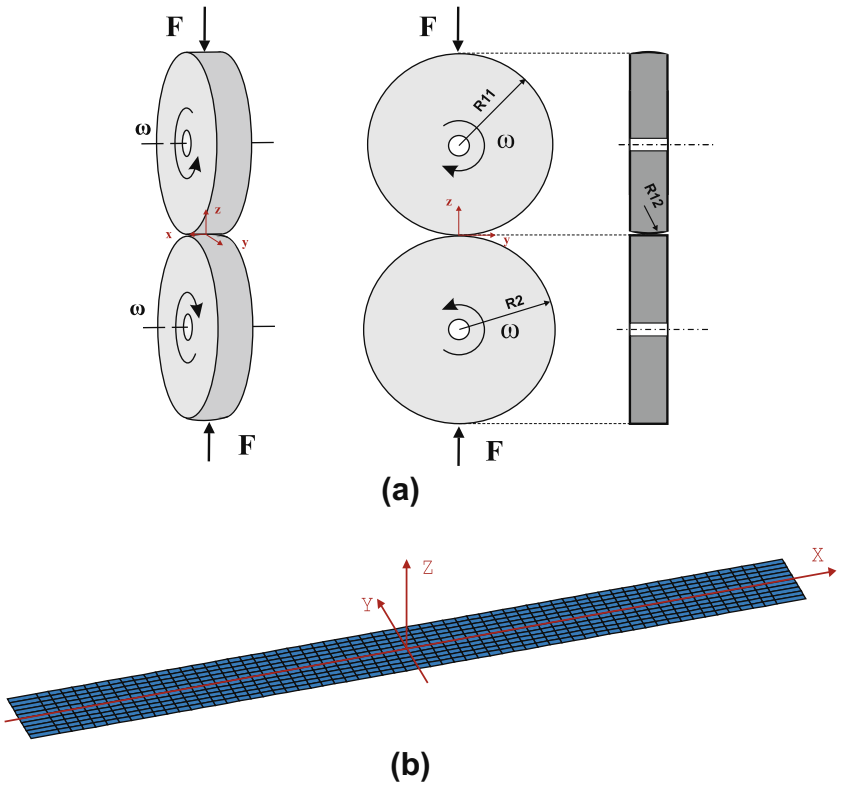

Fig. 11. (a) Twin disc rolling-contact problem. (b) Boundary elements mesh details around the contact zone.

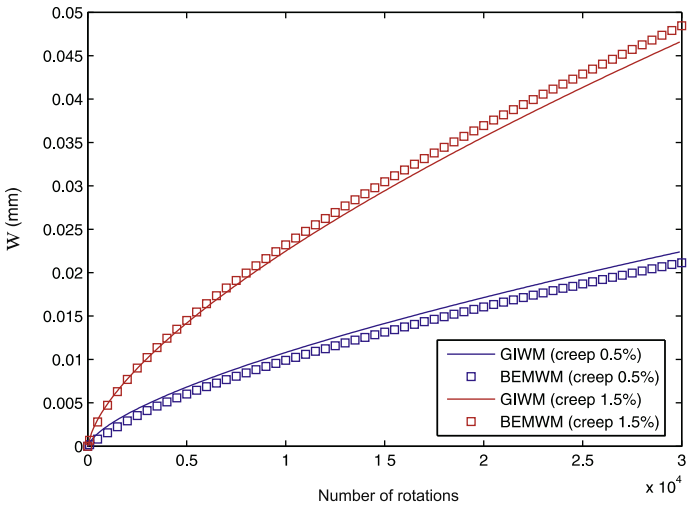

Fig. 12. Wear depth evolution for a normal load of 300 N. Comparison between GIWM and the BEM wear model (BEMWM).

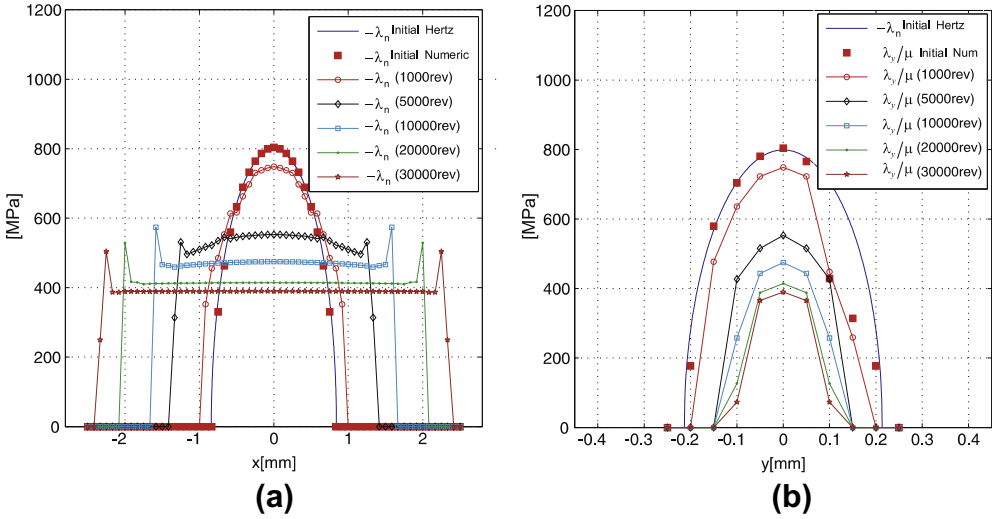

Fig. 13. (a) Normal contact pressure evolution on $y = 0$. (b) Tangential contact traction evolution on $x = 0$.

The main advantage of this BEM formulation is that allows to compute the contact traction evolution and distribution on the contact zone during the wear process, what it is important for general fretting-wear and fretting-fatigue studies, using a very reduced number of degrees of freedom on the model and obtaining a good accuracy. Fig. 13a and b shows the contact tractions evolution from Hertz–Carter distributions, on planes $y = 0$ and $x = 0$, respectively, for a *Creep* = 0.5%, with the number of rotations.

Considering that the hardness of disc 2 is two times the hardness of disc 1, according with (19), the maximum wear depth evolution of each solid is the evolution presented on Fig. 14a for the creep values: *Creep* = 0.5% and *Creep* = 1.5%. After 30,000 revolutions, the solids profiles are plotted on Fig. 14b.

Finally, we have extended the acceleration strategy proposed by Strömbeg (1997) on FEM fretting problems, to 3D rolling-contact problems. This strategy consists of using a fictitious wear coefficient ($k_w = 2 \times 10^{-4}$ MPa^{-1}), what leads to a fictitious wear depth increment, what allows to reduce by one hundred, the cpu times, without loss of accuracy, as Fig. 15 shows for the creep values: 0.5% (a) and 1.5% (b).

7. Conclusions

This work presents a new BEM based methodology for wear simulation on 3D contact and rolling-contact problems. The material loss of the bodies is modeled using the Holm–Archard's linear wear law. The methodology is applied to consider wear on different kind of contact conditions: fretting, sliding wear and rolling-contact. The results obtained present a very good agreement with previous numerical and semi-analytical ones presented in the literature. In this kind of solids mechanical interaction problems, the BEM reveals to be a very suitable numerical method, considering only the degrees of freedom involved on the problem (those on the solids surfaces), and obtaining a very good accuracy on contact tractions with a reduced number of elements. Besides these advantages of the formulation, we have to add that is a 3D formulation, what it is important for general fretting-wear and fretting-fatigue studies. Furthermore, the proposed algorithm of resolution is easy of programming, and can be accelerated, allowing to obtain a very important reductions on wear simulations times. So the proposed methodology is a useful and efficient numerical tool for wear computing on 3D problems.

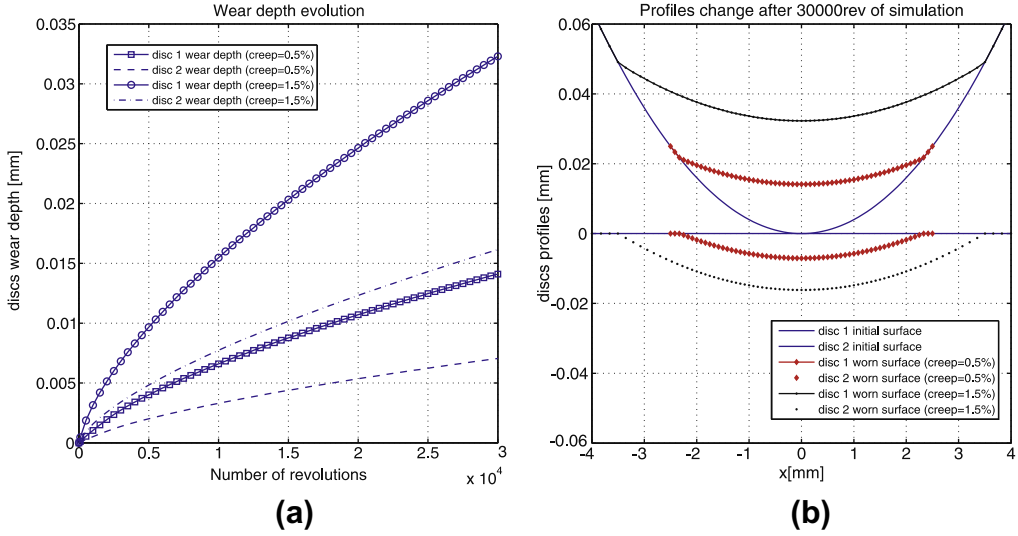

Fig. 14. (a) Maximum wear depth evolution on every disc. (b) Discs profiles after 30,000 revolutions for a creep of: 0.5 % and 1.5%.

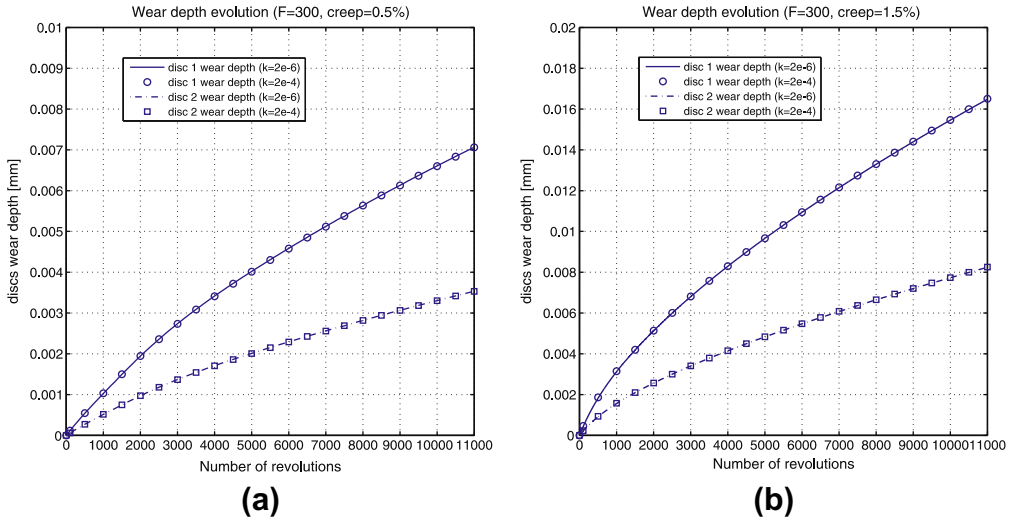

Fig. 15. Maximum wear depth evolution on every disc for a creep of: (a) 0.5% and (b) 1.5%, computed using the real wear coefficient ($k_w = 2 \times 10^{-6}\,\mathrm{MPa}^{-1}$) and a fictitious wear coefficient ($k_w = 2 \times 10^{-4}\,\mathrm{MPa}^{-1}$).

Acknowledgements

This work was co-funded by the DGICYT of *Ministerio de Ciencia y Tecnología*, Spain, research project DPI2006-04598, and by the *Consejería de Innovación Ciencia y Empresa de la Junta de Andalucía*, Spain, research projects P05-TEP-00882 and P08-TEP-03804.

References

Abascal, R., Rodríguez-Tembleque, L., 2007. Steady-state 3D rolling-contact using boundary elements. Commun. Numer. Methods Eng. 33, 905–920.
Alart, P., Cournier, A., 1991. A mixed formulation for frictional contact problems prone to Newton like solution methods. Comput. Methods Appl. Mech. Eng. 92, 353–375.
Aliabadi, M.H., 2002. The Boundary Element Method. Applications in Solids and Structures, vol. 2. John Wiley & Sons.
Archard, J.F., 1953. Contact and rubbing of flat surfaces. J. Appl. Phys. 24, 981–988.
Brebbia, C.A., Dominguez, J., 1992. Boundary Elements: An Introductory Course, second ed. Computational Mechanics Publications, John Wiley & Sons.
Christensen, P.W., Klarbring, A., Pang, J., Strömbeg, N., 1998. Formulation and comparison of algorithms for frictional contact problems. Int. J. Numer. Eng. 42 (1), 145–173.
De Arizon, J., Verlinden, O., Dehombreux, P., 2007. Prediction of wheel wear in urban railway transport: comparison of existing models. Vehicle Syst. Dyn. 45, 849–866.
Enblom, R., Mats, B., 2005. Simulation of railway wheel profile development due to wear-influence of disc braking and contact environment. Wear 258, 1055–1063.
González, J.A., Abascal, R., 1998. Using the boundary element method to solve rolling contact problems. Eng. Anal. Bound. Elem. 21, 392–395.
González, J.A., Abascal, R., 2000. An algorithm to solve coupled 2D rolling contact problems. Int. J. Numer. Methods Eng. 49 (9), 1143–1167.
González, J.A., Abascal, R., 2002. Solving 2D transient rolling contact problems using the BEM and mathematical programming techniques. Int. J. Numer. Methods Eng. 53 (4), 843–875.
Hegadekatte, V., Kurzenhäuser, S., Kraft, O., 2008. A predictive modeling scheme for wear in tribometers. Tribol. Int. 41, 1020–1031.
Holm, R., 1946. Electric Contacts. Almquist and Wiksells Akademiska Handböcker, Stockholm.
Ireman, P., Klarbring, A., Strömbeg, N., 2003. A model of damage coupled to wear. Int. J. Solids Struct. 40, 2957–2974.
Jendel, T., 2002. Prediction of wheel profile wear-comparisons with field measurements. Wear 253, 89–99.
Johansson, L., 1994. Numerical simulation of contact pressure evolution in fretting. J. Tribol. 116, 247–254.
Johnson, K.L., 1985. Contact Mechanics. Cambridge University Press, Cambridge.
Kalker, J.J., 1990. Three-dimensional Elastic Bodies in Rolling Contact. Kluwer Academic Press, Dordrecht.
Landers, J.A., Taylor, R.L., 1985. An Augmented Lagrangian formulation for the finite element solution of contact problems. Rept. No. UCB/SESM-85/09, Department of Civil Engineering, University of California, Berkeley.
Laursen, T.A., 2002. Computational Contact and Impact Mechanics. Springer, England.
Lee, Choon Yeol, Tian, Li Si, Bae, Joon Woo, Chai, Young Suck, 2009. Application of influence function method on the fretting wear of tube-to-plane contact. Tribol. Int. 42, 951–957.
Meng, H., 1994. Wear Modelling: Evaluation and Categorisation of Wear Models. University of Michigan.
Olofsson, U., Andersson, S., Björklund, S., 2000. Simulation of mild wear in boundary lubricated spherical roller thrust bearing. Wear 241, 180–185.
Põdra, P., Andersson, S., 1999a. Simulating sliding wear with finite element method. Tribol. Int. 32, 71–81.
Põdra, P., Andersson, S., 1999b. Finite element analysis wear simulation of a conical spinning contact considering surface topography. Wear 224, 13–21.
Rabinowicz, E., 1995. Friction and Wear of Materials, second ed. Wiley, New York.
Rodríguez-Tembleque, L., Abascal, R., 2010. A 3D FEM–BEM rolling contact formulation for unstructured meshes. Int. J. Solids Struct. 47, 330–353.
Sfantos, G.K., Aliabadi, M.H., 2006a. Application of BEM and optimization technique to wear problems. Int. J. Solids Struct. 43, 3626–3642.
Sfantos, G.K., Aliabadi, M.H., 2006b. Wear simulation using an incremental sliding boundary element method. Wear 260, 1119–1128.
Sfantos, G.K., Aliabadi, M.H., 2007. A boundary element formulation for three-dimensional sliding wear simulation. Wear 262, 672–683.
Simo, J.C., Laursen, T.A., 1992. An augmented Lagragian treatment of contact problems involving friction. Comput. Struct. 42, 97–116.
Simo, J.C., Wriggers, P., Taylor, R.L., 1985. A perturbed Lagrangian formulation for the finite element solution of contact problems. Comput. Methods Appl. Mech. Eng. 50, 163–180.
Strömbeg, N., 1997. An augmented lagrangian method for fretting problems. Eur. J. Mech. A/Solids 16 (4), 573–593.
Strömbeg, N., 1999. A Newton method for three-dimensional fretting problems. Int. J. Solids Struct. 36 (4), 2075–2090.
Strömbeg, N., Johansson, L., Klarbring, A., 1996. Derivation and analysis of a generalized standard model for contact, friction and wear. Int. J. Solids Struct. 33 (13), 1817–1836.
Telliskivi, T., 2004. Simulation of wear in a rolling–sliding contact by a semi-Winkler model and the Archard's wear law. Wear 256, 817–831.
Telliskivi, T., Olofsson, U., 2004. Wheel–rail wear simulation. Wear 257, 1145–1153.
Wriggers, P., 2002. Computational Contact Mechanics. West Sussex, England.
Wriggers, P., Simo, J.C., Taylor, R.L., 1985. Penalty and augmented Lagragian formulations for contact problems. In: Proceedings of the NUMETA'85 Conference, Swansea.